Journal of the Optical Society of America A
OPTICS, IMAGE SCIENCE, AND VISION

Speckle-illumination averaged wide-field reflection phase microscopy

T. S. ATHIRA,[1,*] PRAMOD PANCHAL,[2] RAKESH K. SINGH,[3] AND DINESH N. NAIK[4]

[1]Department of Physics, Govt K.N.M. Arts and Science College, Thiruvananthapuram, Kerala 695524, India
[2]ITCC, Indian Institute of Astrophysics, Koramangala Block-II, Bangalore, India
[3]Laboratory of Information Photonics and Optical Metrology, Department of Physics, Indian Institute of Technology (Banaras Hindu University), Varanasi 221005, Uttar Pradesh, India
[4]Applied and Adaptive Optics Laboratory, Department of Physics, Indian Institute of Space Science and Technology, Thiruvananthapuram, Kerala 695547, India
*athiratsoptics@gmail.com

Received 23 December 2025; revised 10 April 2026; accepted 18 April 2026; posted 21 April 2026; published 5 May 2026

An experimental scheme solely employing scalar optics to achieve speckle-illumination averaged wide-field reflection phase microscopy is proposed. The experimental setup utilizes a Sagnac-Linnik Michelson interferometer design, providing greater stability compared to conventional setups. The 3-D/phase imaging of the sample is achieved with reduced speckle noise, wider field of view, and improved resolution.

https://doi.org/10.1364/JOSAA.587767

1. INTRODUCTION

In conventional off-axis holography-based phase measurement schemes, a uniform reference field is generally preferred due to simplicity and the ability to reconstruct complex amplitude from a single recording [1,2]. The reference field is maintained with a uniform cleaner intensity profile that requires the laser field to pass through the spatially filtering assemblies. Moreover, due to limited beam size and field propagation through aperture limited optical elements, any spatial variation in amplitude and phase of the reference field needs to be quantified prior to the recording of the hologram with samples. Also, in microscopic techniques based on holography, spatial resolution is limited by beam size as well as numerical aperture of the imaging system.

To improve resolution in holographic microscopy, the conventional interferometric setup with a planar reference field is modified using various illumination mechanisms such as structured illumination, swept angle illumination, and speckle field illumination [3]. In structured illumination methods, expensive display devices such as spatial light modulators are used to produce fringes of different orientations for illuminating the object and extracting microscopic details [4–6]. However, these methods are susceptible to artifacts such as Moiré fringes, misalignment sensitivity, and aberrations. Also the holographic experimental setups employing swept angle illumination/synthetic aperture imaging involve movement of optical components to illuminate the object at various angles demanding complex computational processing [7,8]. Meanwhile in digital holographic microscopy techniques with swept-source, the wavelength of low-coherence source or tunable laser diode is tuned across a range to produce a series of interferograms, which are then analyzed to extract object features [9]. Although it reduces unwanted interference artifacts and enhances resolution, the use of motorized devices in swept-source methods adds complexity, increases costs, and presents challenges for the practical application of the experiment.

On the other hand, allowing a statistically correlated dynamic speckle field as the reference, the influence of the reference field in the reconstructed complex amplitude of the sample is shown to average out. In addition, the use of the same speckle field as the illuminating field, apart from averaging of speckle noise in the reconstructed complex amplitude, provides wider field of view and improved resolution compared to the case where a plane wave is used as illumination field [10–12].

A. Resolution in Microscopic Imaging System

The experimental setups that achieve microscopic imaging mainly consist of two microscopes, one for illuminating the sample and other for collecting the field from the sample, as shown in Fig. 1. The numerical aperture of the microscopic objectives decides the resolution of the experimental setup. The spatial resolution of holographic microscopy as explained in [5] is given by

$$\delta = \frac{k_1 \lambda}{\mathrm{NA}_{\mathrm{MO}_{\mathrm{ill}}} + \mathrm{NA}_{\mathrm{MO}_{\mathrm{col}}}}, \quad (1)$$

where λ is wavelength of the light used. k_1 is determined by various experimental parameters. Theoretically, the parameter

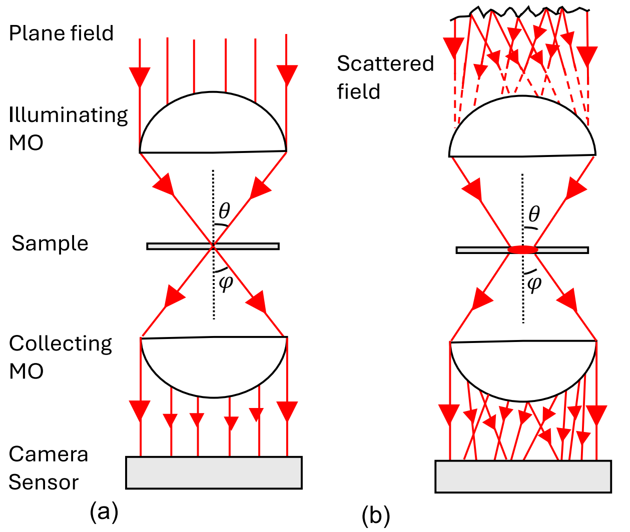

Fig. 1. Imaging using microscopic objectives: (a) plane field illumination and (b) speckle field illumination.

k_1 is 1.22, as given by Rayleigh's resolution criterion, assuming that all other experimental factors influencing the system are neglected. The $NA_{MO_{ill}} = \sin\theta$ and $NA_{MO_{col}} = \sin\phi$ are numerical apertures (NA) of illuminating and collecting microscopic objectives (MO) respectively. As previously mentioned, traditional microscopic imaging projects a uniform, unscattered plane field onto the MOs, as shown in Fig. 1(a). In contrast, introducing a scattered field into the microscopic imaging system, as depicted in Fig. 1(b), results in the sample interacting with a field having a complex angular spectrum. Scattered light spreads over a wide range of varying angles and intensities, resulting better contrast and enhanced object features compared to plane field illumination.

In an experimental demonstration of phase microscopy using dynamic speckle illumination, polarization optics were extensively used [10]. A polarizing beam splitter, followed by wave plates, was used for beam splitting and recombining with distinguishability between sample and reference fields in a Michelson interferometer. A combination of diffraction grating and multiple polarizers was used to introduce carrier frequency in the recorded interferogram. By doing so, the scheme utilized the polarization degree of freedom, leaving only a scalar field to probe the sample information.

We propose an experimental scheme solely employing scalar optics to achieve speckle-illumination averaged wide-field reflection phase microscopy, keeping all the advantages of the scheme such as reduced speckle noise, wider field of view, improved resolution, and normal illumination/collection of the light to/from the sample. In this sense, all the optical elements except for the lens at the output of the system are centered with respect to the optical field propagation direction. Avoiding any polarization optics in the scheme, the polarization degree of freedom may potentially be utilized to probe birefringent/optically active samples as well. The proposed scheme utilizes a simple and efficient computational technique, the Fourier transform method of fringe analysis in image processing, for reconstructing the object.

2. EXPERIMENTAL SETUP AND RESULTS

The proposed scheme is realized using an experimental design comprising of a Sagnac interferometer followed by a Linnik-type Michelson interferometer [13] as shown in Fig. 2. The light from the He–Ne laser (wavelength, $\lambda = 632.8$ nm) is collimated using two microscope objectives MO1 and MO2 of the same magnification (10X). In the absence of the rotating ground glass in the common focal region of the two microscope objectives, the collimated laser beam of lateral size 1 mm enters into a Sagnac interferometer consists of mirrors M1 and M2. The beam splitter BS1 splits the beam into two, and the separation between them is controlled by the position of the mirrors M1 and M2. Thus the two laterally separated beams are allowed to enter into a Linnik-type Michelson Interferometer. The Linnik-type interferometer is composed of two objective lenses MO3 and MO4 of magnification 5X in conjunction with mirrors M3 and M4. The apertures of microscopic objectives are adjusted to allow the passage of only one field toward the respective mirrors. The fields reflected from the mirrors combine at the beam splitter BS2. The fields overlap at the CCD (charge-coupled device) plane with the help of the lens where they interfere to produce fringes which are parallel due to the tilt between the interfering beams.

A ground glass (GG) is placed between the microscopic objectives MO1 and MO2, which scrambles the intensity at input. The Sagnac interferometer shifts the two copies of the speckle field laterally and feeds it into Michelson interferometer. To observe speckle interference, the lengths of the arms of the Michelson interferometer are adjusted to be exactly equal. This ensures that the fields reflecting from both mirrors exhibit identical speckle intensity distributions. The fields interfere to produce parallel fringes along with speckles as shown in Fig. 3(a). The speckles in the interferograms act as noises and hinder the reconstruction of object information. However, with appropriate speckle suppression methods, the interferograms can be cleaned out. For this, the ground glass is rotated to alter the intensity distribution of the speckle fields. The ground glass controller is then, triggered to the CCD (model: PCO pixel fly). Therefore, uncorrelated speckle patterns generated by the rotation of ground glass result in various interferograms, which are subsequently captured by the CCD. CCD records around 200 interferograms corresponding to each uncorrelated

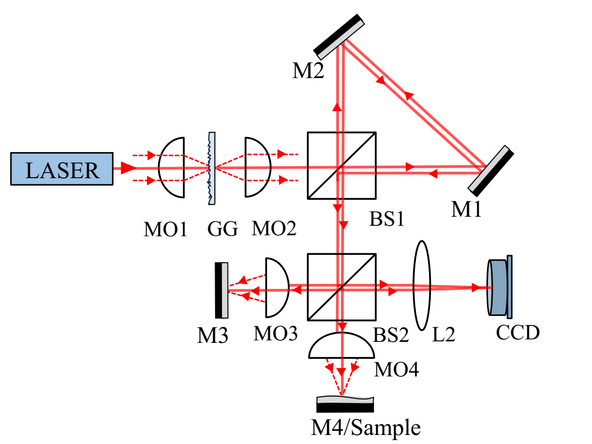

Fig. 2. Experimental setup.

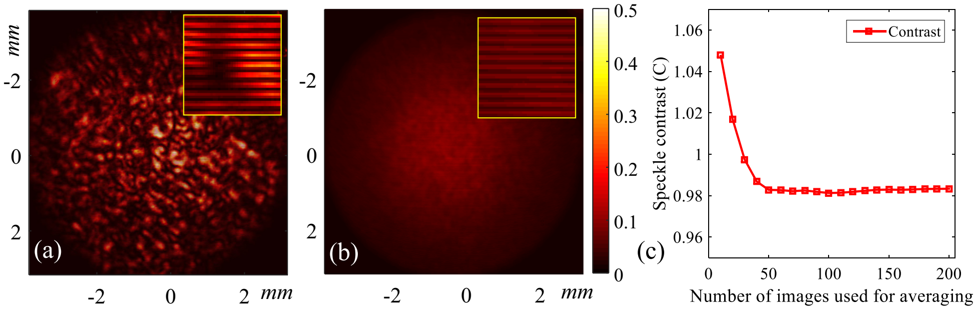

Fig. 3. (a) Interferogram with speckles. (b) Interferogram obtained after removing the speckles. (c) Speckle contrast versus the number of images used for averaging.

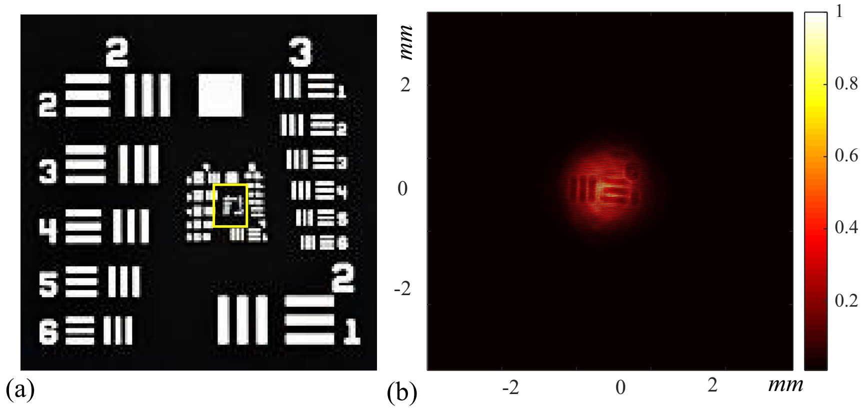

Fig. 4. (a) Details of USAF used as the sample. The region of the sample used for the investigation is shown in the yellow box. (b) Interferogram with plane-wave illumination/reference.

speckle patterns. Though the interferograms are uncorrelated by speckle intensities, they have identical parallel fringe intensity distribution. Hence the intensity of ith interferogram, $I^i(x)$, is obtained as

$$I^i(x) = I^i_{\text{speckle}}(x) \times I_{\text{parallel}}(x), \tag{2}$$

where $I^i_{\text{speckle}}(x)$ is the intensity of speckles in the ith interferogram obtained. $I_{\text{parallel}}(x)$ represents the common hidden parallel fringes of these interferograms. These interferograms are added and averaged out to suppress the speckles:

$$\bar{I}(x) = \frac{1}{N}\sum_{i=1}^{N} I^i(x) = I_{\text{parallel}}(x)\frac{1}{N}\sum_{i=1}^{N} I^i_{\text{speckle}}(x), \tag{3}$$

$$\bar{I}(x) = I_{\text{parallel}}(x) \times \overline{I_{\text{speckle}}}(x), \tag{4}$$

where $\overline{I_{\text{speckle}}}(x)$ is mean speckle intensity and spatially uniform. Thus speckles are effectively averaged out leaving only parallel fringes for retrieving the information of sample. If we add N number of uncorrelated speckle intensities, the resulting intensity will have reduced speckle contrast given by the equation [14]

$$C = \frac{\sigma_I}{\overline{I_{\text{speckle}}}} = \frac{1}{\sqrt{N}}, \tag{5}$$

where σ_I is standard deviation of the resultant speckle intensity distribution. By selecting appropriate number of images for averaging (approximately 200), the interferogram with clear parallel fringes void of speckles similar to one shown in Fig. 3(b) is obtained. The effect of the number of images used for averaging on the speckle contrast is illustrated in Fig. 3(c). Using fewer than 50 images results in speckle noise. Therefore, 200 images were selected for averaging, as the speckle contrast reaches a constant value of approximately 0.983.

The mirror M4 is replaced by the sample: a 1 in. negative USAF 1951 test chart. The sample is imaged at the camera plane. The sample is depicted in Fig. 4(a), with the region highlighted by the yellow box used as the object. The ground glass is removed and interferograms with direct/plane fields are captured as one shown in Fig. 4(b).

The interferogram with speckle field illumination is obtained for the same sample, after inserting ground glass, as in Fig. 5(a). It is then averaged out to get smooth parallel fringes as shown in Fig. 5(b). As observed in Figs. 5(b) and 4(b), the area of illumination is larger with the use of ground glass. On the other hand, with the plane field illumination, the size of beam limits the information of object. When the ground glass is inserted, the beam size gets enlarged, illuminating more area of object, giving more information about the object. The size of beam, in this case, can be varied by shifting the ground glass in the longitudinal direction between the microscopic objectives MO1 and MO2.

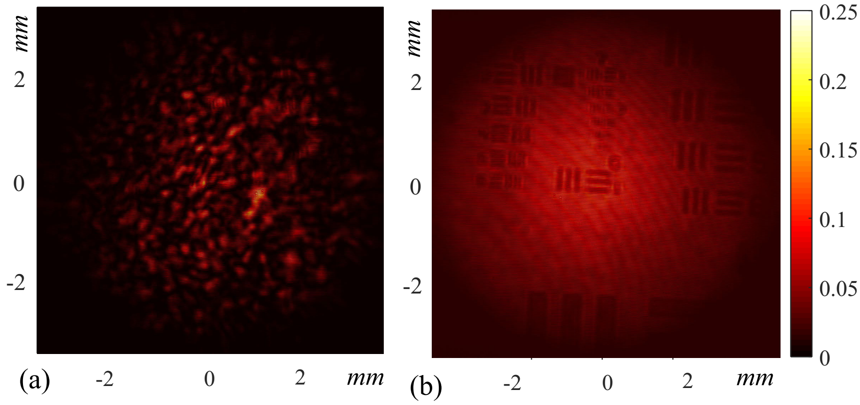

Fig. 5. (a) Interferogram containing object information with speckles. (b) Interferogram obtained after removing the speckles.

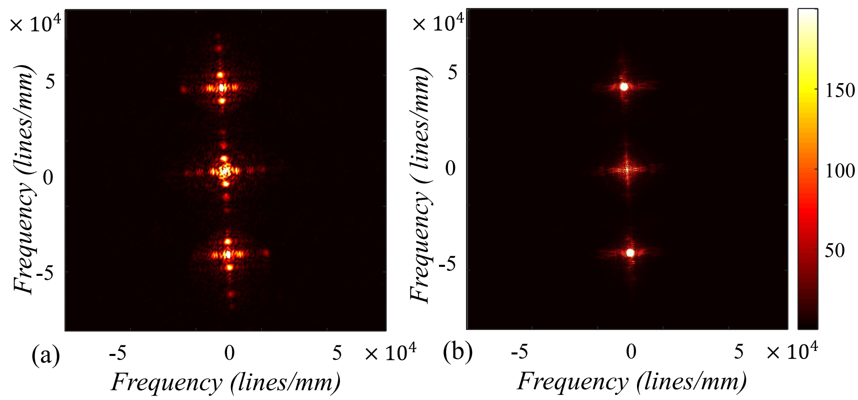

Fig. 6. (a) Absolute of Fourier transform of interferogram shown in Fig. 5(b). (b) Absolute of Fourier transform of interferogram shown in Fig. 4(b).

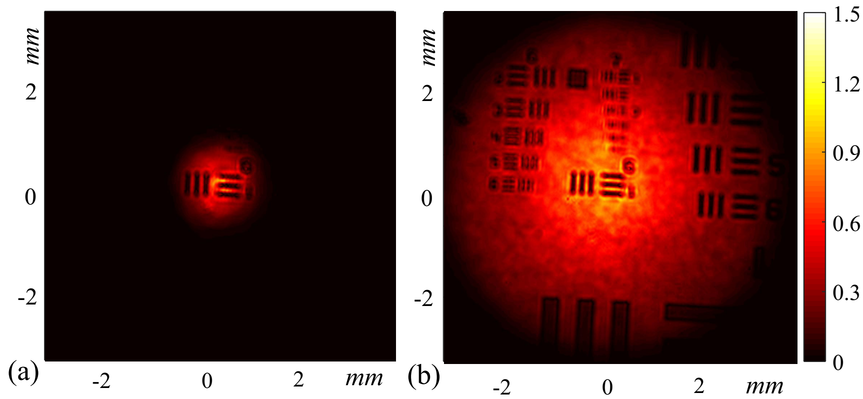

Fig. 7. Defocused image of the sample reconstructed from the FT method of fringe analysis (equivalent to the direct image if recorded without reference field): (a) with plane-wave illumination and (b) with speckle field illumination.

After acquiring interferograms in both cases, the object information is extracted using the Fourier transform method for fringe analysis [15]. Figures 6(a) and 6(b) show the intensity of Fourier transform of interferograms shown in Figs. 5(b) and 4(b), respectively. Reconstructed fields are defocused as the camera plane is slightly away from the focal plane of lens L2. The defocused images obtained through Fourier fringe analysis for both plane field illumination and speckle field illumination are shown in Figs. 7(a) and 7(b). The field at the camera plane is back propagated to the focal plane of the lens L2 through computational methods to obtain focused object information, as shown in Figs. 8(a) and 8(b).

In order to investigate resolution capabilities, the region of the USAF chart with the smallest lettering is illuminated, as depicted in Fig. 9. As the illuminating and collecting MOs are same in the experimental setup, the resolution of the system is found as

$$\delta = \frac{k_1 \lambda}{2\mathrm{NA}_{\mathrm{MO4}}}, \tag{6}$$

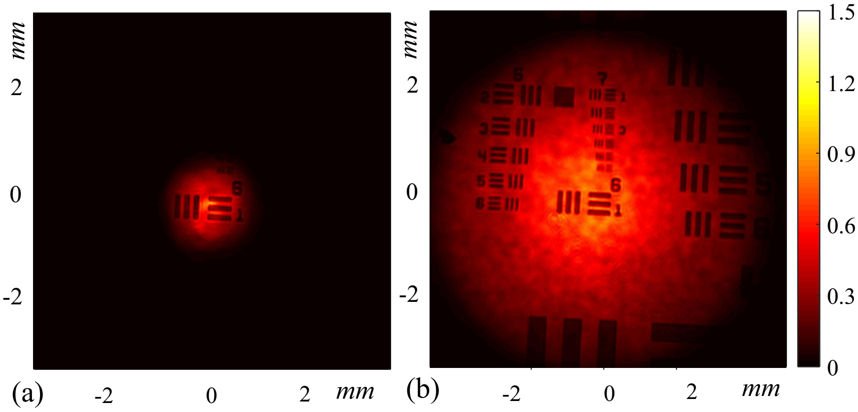

Fig. 8. Focused image of the sample obtained through propagation: (a) with plane-wave illumination and (b) with speckle field illumination.

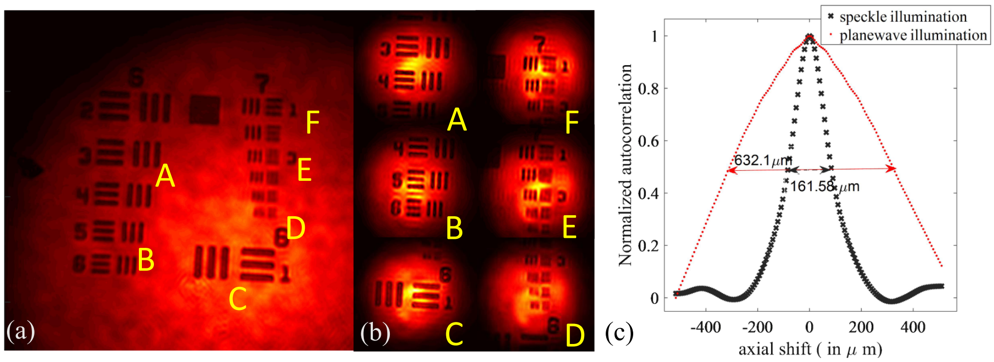

Fig. 9. Comparison of resolution: (a) reconstructed intensity with speckle field illumination; (b) collage of reconstructions of different regions of USAF target using plane-wave illumination; and (c) normalized autocorrelation functions of the speckle field and the plane-wave field.

where NA_{MO4} is the numerical aperture of MO4. The theoretical resolution limit of the current setup having MO of 5X magnification and $NA = 0.10$ becomes 3.86 μm. The limit can reach the nanometer scale, depending on the numerical aperture of the microscope objective (MO) and the laser wavelength used. For an MO with 60X magnification and an 800 nm wavelength, a resolution of up to 490 nm can be achieved. However, higher magnification MOs can cause challenges such as a smaller field of view, high sensitivity to aberrations and vibrations, and difficulty in alignment. Figure 9(a) illustrates the reconstructed intensity of the sample under speckle illumination, while Fig. 9(b) shows a collage of reconstructed intensities of various regions within the same area of interest, acquired through plane-wave illumination. In both scenarios, vertical lines in the USAF chart exhibit better resolution than horizontal lines. This discrepancy occurs because of the initial alignment of parallel fringes in the horizontal direction. As a result, the detailing of the sample in the horizontal direction is resolved less effectively compared to other orientations. The lines in the regions D, E, and F are resolved well in the case of speckle illumination. However, with plane-wave illumination, the horizontal lines in the region D, E, and F, are seen blurred. Vertical lines with widths up to 2.76 μm and horizontal lines with width up to 3.48 μm are seen resolved in the reconstruction with speckle illumination. With plane field illumination, vertical lines with a width of up to 3.10 μm and horizontal lines with a width up to 4.38 μm can only be resolved visibly.

The best achievable resolution of the given optical system is evaluated using the axial full width at half-maximum of the autocorrelation functions, as shown in Fig. 9(c). The comparison shows that the Gaussian peak width in the speckle pattern is roughly one-fifth of that obtained with plane-wave illumination. Hence, the proposed method provides significantly better resolution than conventional holography. To evaluate the resolution corresponding to the different modulations present in the image, we use modulation transfer function (MTF) analysis. The various modulation patterns (both vertical and horizontal line features) in Fig. 8 are cropped individually, and the MTF is computed for each selected region. The resulting MTFs are then plotted as a function of spatial frequency, expressed in lines per millimeter (lp/mm), as shown in Fig. 10(a). We set the MTF at 20% as the resolution criterion of the experimental setup. We found that our experimental setup is able to resolve 152.8 vertical lp/mm and 193.8 horizontal lp/mm. This confirms that our system provides better resolution for vertical lines than for horizontal lines. The fluctuations in MTF values corresponding to 55–125 lp/mm may be due to aberrations, as the corresponding regions lie away from the centre of the image. The MTF at a particular frequency, say 64 lp/mm, was studied for different numbers of images used in averaging to understand the effect of averaging on image resolution. It is observed that as the number of images increases, the MTF value approaches a plateau, as shown in Fig. 10(b). Additionally, the length of the error bars decreases as the number of images increases. This

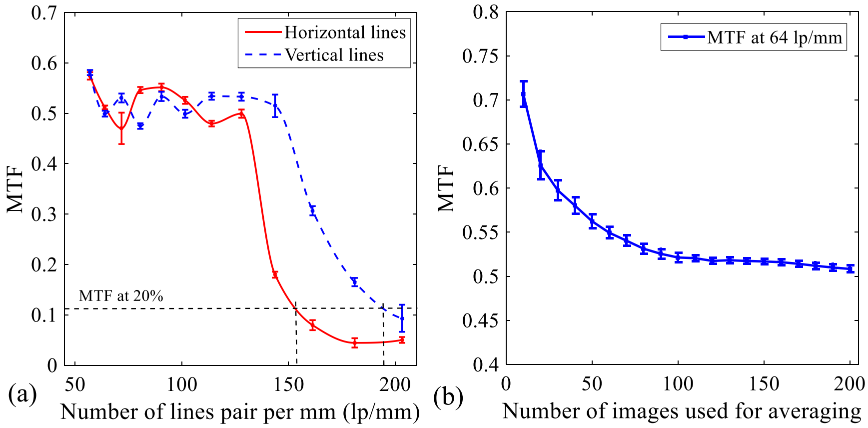

Fig. 10. (a) MTF for horizontal and vertical lines plotted against the number of line pairs per millimeter (lp/mm), with error bars. (b) MTF at 64 lp/mm plotted against the number of images used for averaging.

indicates that averaging effectively reduces speckle noise and enhances the accuracy of the resolution.

3. CONCLUSION

In conclusion, the proposed experimental setup can have potential applications in holographic techniques with speckle field illumination, offering improved resolution and a broader field of view within an optical environment free from aberration and polarization effects. Unlike optical coherence tomography systems that employ low-coherence sources and are susceptible to dispersion, our experiment uses a narrow-linewidth laser speckle source that mimics low coherence, making the method largely insensitive to dispersion. The resolution can reach the nanoscale using MOs with high numerical aperture and longer laser wavelengths. The precise alignment of the components in the experimental setup ensures the maximum visibility of interference fringes during the speckle illumination. The arm lengths of the Michelson interferometer have to be exactly equal to observe the fringes at the image plane, eliminating chances of getting aberrated fields. Thus, the proposed optical setup guarantees an aberration-free optical system, unlike most of the conventional holographic setups employing structured illumination/swept angle illumination. The potential of our experimental setup to resolve depth sectioning in both normal and birefringent samples will be investigated in the future.

Disclosures. The authors declare no conflicts of interest.

Data availability. Data underlying the results presented in this paper are not publicly available at this time but may be obtained from the authors upon reasonable request.

REFERENCES

1. D. Gabor, W. E. Kock, and G. W. Stroke, "Holography: the fundamentals, properties, and applications of holograms are reviewed," Science **173**, 11–23 (1971).
2. U. Schnars, C. Falldorf, J. Watson, *et al.*, *Digital Holography* (Springer, 2015).
3. C. J. Schwarz, Y. Kuznetsova, and S. R. J. Brueck, "Imaging interferometric microscopy," Opt. Lett. **28**, 1424–1426 (2003).
4. R. V. Vinu, Z. Chen, J. Pu, *et al.*, "Speckle-field digital polarization holographic microscopy," Opt. Lett. **44**, 5711–5714 (2019).
5. P. Gao, G. Pedrini, and W. Osten, "Structured illumination for resolution enhancement and autofocusing in digital holographic microscopy," Opt. Lett. **38**, 1328–1330 (2013).
6. K. Wen, Z. Gao, R. Liu, *et al.*, "Structured illumination phase and fluorescence microscopy for bioimaging," Appl. Opt. **62**, 4871–4879 (2023).
7. C. Yuan, G. Situ, G. Pedrini, *et al.*, "Resolution improvement in digital holography by angular and polarization multiplexing," Appl. Opt. **50**, B6–B11 (2011).
8. S. A. Alexandrov, T. R. Hillman, T. Gutzler, *et al.*, "Synthetic aperture fourier holographic optical microscopy," Phys. Rev. Lett. **97**, 168102 (2006).
9. S. Chen, J. Ryu, K. Lee, *et al.*, "Swept source digital holographic phase microscopy," Opt. Lett. **41**, 665–668 (2016).
10. Y. Choi, P. Hosseini, W. Choi, *et al.*, "Dynamic speckle illumination wide-field reflection phase microscopy," Opt. Lett. **39**, 6062–6065 (2014).
11. A. Ahmad, N. Jayakumar, and B. S. Ahluwalia, "Demystifying speckle field interference microscopy," Sci. Rep. **12**, 10869 (2022).
12. Y. Liu, P. Bu, M. Jiao, *et al.*, "Dynamic speckle illumination digital holographic microscopy by doubly scattered system," Photonics **8**, 276 (2021) .
13. P. Kühnhold, W. Xie, and P. Lehmann, "Comparison of michelson and linnik interference microscopes with respect to measurement capabilities and adjustment efforts," Proc. SPIE **8788**, 684–694 (2013).
14. J. W. Goodman, "Some fundamental properties of speckle *," J. Opt. Soc. Am. **66**, 1145–1150 (1976).
15. M. Takeda, H. Ina, and S. Kobayashi, "Fourier-transform method of fringe-pattern analysis for computer-based topography and interferometry," J. Opt. Soc. Am. **72**, 156–160 (1982).